The Astrophysical Journal Letters, 900:L34 (6pp), 2020 September 10 https://doi.org/10.3847/2041-8213/abac56

Dragon's Lair: On the Large-scale Environment of BL Lac Objects

F. Massaro[1,2,3,4], A. Capetti[2], A. Paggi[1,2,3], R. D. Baldi[1,5], A. Tramacere[6], I. Pillitteri[7], and R. Campana[8]
[1] Dipartimento di Fisica, Università degli Studi di Torino, via Pietro Giuria 1, I-10125 Torino, Italy
[2] INAF-Osservatorio Astrofisico di Torino, via Osservatorio 20, I-10025 Pino Torinese, Italy
[3] Istituto Nazionale di Fisica Nucleare, Sezione di Torino, I-10125 Torino, Italy
[4] Consorzio Interuniversitario per la Fisica Spaziale, via Pietro Giuria 1, I-10125 Torino, Italy
[5] Department of Physics and Astronomy, University of Southampton, Highfield, SO17 1BJ, UK
[6] University of Geneva, Chemin d'Ecogia 16, Versoix, CH-1290, Switzerland
[7] INAF-Osservatorio Astronomico di Palermo G.S. Vaiana, Piazza del Parlamento 1, I-90134, Italy
[8] INAF/OAS, via Piero Gobetti 101, I-40129, Bologna, Italy
Received 2020 June 13; revised 2020 July 18; accepted 2020 July 30; published 2020 September 9

Abstract

The most elusive and extreme subclass of active galactic nuclei (AGNs), known as BL Lac objects, shows features that can only be explained as the result of relativistic effects occurring in jets pointing at a small angle with respect to the line of sight. A longstanding issue is the identification of the BL Lac parent population with jets oriented at larger angles. According to the "unification scenario" of AGNs, radio galaxies with low luminosity and an edge-darkened radio morphology are the most promising candidate parent population of BL Lacs. Here we compare the large-scale environment, an orientation-independent property, of well-defined samples of BL Lacs with samples of radio galaxies all lying in the local universe. Our study reveals that BL Lacs and radio galaxies live in significantly different environments, challenging predictions of the unification scenario. We propose a solution to this problem proving that large-scale environments of BL Lacs are statistically consistent with those of compact radio sources, known as FR 0s, and share similar properties. This implies that highly relativistic jets are ubiquitous and are the natural outcome of the accretion of gas into the deep gravitational potential well produced by supermassive black holes.

Unified Astronomy Thesaurus concepts: Relativistic jets (1390); Astrostatistics (1882); Active galaxies (17); Radio galaxies (1343); Galaxy clusters (584); BL Lacertae objects (158)

Supporting material: machine-readable table

1. Introduction

Since the early 1970s, extended radio galaxies have been divided into two main types based on their radio morphology: edge-darkened (FR I type) and edge-brightened (FR II type) sources (Fanaroff & Riley 1974). For decades this dichotomy was linked to their radio power and their large-scale environments as follows: FR Is generally inhabit galaxy-rich environments and are members of groups or galaxy clusters, while FR IIs are more isolated (see, e.g., Zirbel 1997). Radio galaxies were also classified on the basis of their optical spectra (Hine & Longair 1979) as high- or low-excitation radio galaxies (HERGs and LERGs, respectively). While LERGs can show both FR I or FR II radio morphology (see e.g., Laing et al. 1994), HERGs appear to be, almost exclusively, FR IIs (see also Heckman & Best 2014).

Furthermore, it is becoming clear that the majority of low-redshift radio galaxies are compact sources. These, known as FR 0s, have typical sizes $\lesssim$10 kpc and are characterized by an LERG spectrum (Baldi et al. 2015) and have recently been shown to live in poorer environments with respect to extended radio sources (Capetti et al. 2020).

On the other hand, BL Lac objects (hereinafter BZBs) are now recognized as the most extreme class of active galactic nuclei (AGNs). Emitting from radio to TeV energies, they constitute the largest population of gamma-ray sources (Abdollahi et al. 2020; Massaro et al. 2015b) and show several peculiar observational properties : flat radio spectra (Healey et al. 2007; Massaro et al. 2013), apparent superluminal motions (Lister et al. 2013), extreme variability up to TeV energies (Aharonian et al. 2007), high radio-to-optical polarization (Pavlidou et al. 2014), peculiar mid-infrared colors (Massaro et al. 2011, 2012a) D'Abrusco et al. 2012), and featureless optical spectra, with only weak emission/absorption features (Stickel et al. 1991). At the 1978 Pittsburgh Conference (Blandford & Rees 1978) proposed to interpret all these features as nonthermal emission arising from particles flowing in a relativistic jet observed at a small angle with respect to the line of sight.

According to the "unification scenario" of radio-loud AGNs, at zeroth order, all jetted AGNs are intrinsically the same but they appear diverse due to different orientations with respect to the line of sight (Urry & Padovani 1995). This idea immediately prompted the quest for the identification of misaligned BZBs. Among radio-loud AGNs, radio galaxies, mainly those belonging to the FR I radio class (Fanaroff & Riley 1974), having low luminosity and an edge-darkened radio morphology, were naturally identified as the BZB parent population, since they also produce relativistic jets extending up to hundreds of kiloparsec scales and lack broad emission lines.

There is a vast literature of tests of the validity of this unification scenario, in particular those performed on the basis of the study of the large-scale environments (see e.g., Villarroel & Korn 2014; Zou et al. 2019), an orientation-independent property of AGNs (Antonucci & Ulvestad 1985). Here we carry out a statistical environmental test of the "unification scenario," comparing a selected sample of BZBs with both (i) FR Is and (ii) LERGs, aiming to verify whether radio galaxies and BZBs inhabit the same galaxy-rich large-scale environments.

We adopt cgs units for numerical results and we assume a flat cosmology with $H_0 = 69.6$ km s^{-1} Mpc^{-1}, $\Omega_M = 0.286$

Table 1
Environmental Parameters for All Sample Analyzed (First 10 Lines)

Sample	Name	R.A. (J2000) (hh:mm:ss.ss)	Decl. (J2000) (hh:mm:ss.ss)	z_{src}	Δz	d_{proj} (kpc)	N_{cn}^{500}	N_{cn}^{1000}	N_{cn}^{2000}
FR0	SDSSJ010852.48–003919.4	01:08:52.48	−00:39:19.40	0.045	0.0012	303.05	2	6	7
FR0	SDSSJ011204.61–001442.4	01:12:04.61	−00:14:42.40	0.044	4.0E−4	556.58	0	1	1
FR0	SDSSJ011515.78+001248.4	01:15:15.78	+00:12:48.40	0.045	2.0E−4	173.27	27	39	39
FR0	SDSSJ015127.10–083019.3	01:51:27.10	−08:30:19.30	0.018	2.0E−4	30.75	12	13	13
FR0	SDSSJ020835.81–083754.8	02:08:35.81	−08:37:54.80	0.034	3.0E−4	413.79	1	2	2
LERG	SDSSJ073014.37+393200.4	07:30:14.37	+39:32:00.40	0.142	0.0011	207.56	1	4	6
LERG	SDSSJ073505.25+415827.5	07:35:05.25	+41:58:27.50	0.087	6.0E−4	758.0	3	4	10
LERG	SDSSJ073719.18+292932.0	07:37:19.18	+29:29:32.00	0.111	0.0034	826.91	1	1	5
LERG	SDSSJ074125.85+480914.3	07:41:25.85	+48:09:14.30	0.12	0.005	1890.54	0	0	1
LERG	SDSSJ074351.25+282128.0	07:43:51.25	+28:21:28.00	0.106	3.0E−4	258.8	4	4	9

Note. Column (1): sample. Column (2): source name. Column (3): right ascension. Column (4): declination. Column (5): redshift. Column (6): difference between the average redshift of cosmological neighbors in 2 Mpc and that of the central source. Column (7): physical distance between the central RG and the average position of cosmological neighbors within 2 Mpc, computed at z_{src}. Columns (8), (9), (10): number of cosmological neighbors within 500, 1000, and 2000 kpc, respectively.
(This table is available in its entirety in machine-readable form.)

and $\Omega_\Lambda = 0.714$ (Bennett et al. 2014), unless otherwise stated, as adopted in previous analyses (see Massaro et al. 2019, 2020; hereafter M19 and M20, respectively).

2. Sample Selection

We combined sources listed in the FR ICAT with those of the sFR ICAT sample for a total of 209 FR Is (Capetti et al. 2017a). The former sample lists FR Is at redshifts $z_{src} \leqslant 0.15$,[9] selected to have a radio structure extending beyond 30 kpc, measured from the location of the host galaxy as seen in the optical band, while the latter includes 14 FR Is with radio emission between 10 and 30 kpc and $z_{src} \leqslant 0.05$. Then we also considered 101 FR IIs, in the same redshift range and all classified as LERGs, collected out of the FR IICAT (Capetti et al. 2017b) to obtain a sample of 310 LERGs. Both FR ICAT and FR IICAT are based on data available in the Sloan Digital Sky Survey (see, e.g., Ahn et al. 2012) and the Faint Images of the Radio Sky at Twenty-cm survey (FIRST; White et al. 1997).

In our analysis we also performed a comparison with 108 FR 0 radio galaxies selected in Baldi et al. (2018). These radio galaxies have all the following properties: (i) $z_{src} < 0.05$; (ii) optical classification as LERGs; (iii) a radio flux density at 1.4 GHz in the FIRST survey above 5 mJy; and (iii) a lack of extended radio emission beyond a few kiloparsecs.

For BZBs we selected only those lying in the same SDSS central footprint and having a firm redshift estimate at $z_{src} \leqslant 0.15$, all from the fifth release of the Roma-BZCAT (Massaro et al. 2015a); this produced a total of 11 sources. Then we also added three more BZBs lying at $z_{src} < 0.15$ that were recently discovered thanks to our optical spectroscopic follow-up campaign of low-energy counterparts for the unidentified γ-ray sources (Massaro et al. 2012b, 2016; de Menezes et al. 2019; Peña-Herazo et al. 2020). Thus, the final sample of BZBs considered in our analysis contains 14 objects in the same redshift bin of radio galaxies.

For a comparison with literature results we also considered BL Lacs-galaxy dominated (BZGs) as listed in the Roma-BZCAT. Adopting the same criteria used for the BZB selection we extracted 41 BZGs lying between $0.02 < z < 0.15$, with 14 out of 41 being associated with a γ-ray source (Abdollahi et al. 2020). BZGs are radio sources whose multifrequency emission exhibits some properties of BL Lacs but appear dominated by the host galaxy contribution, in particular in the optical-ultraviolet energy range. It is not yet clear whether BZGs are all genuine BZBs in a quiescent state, given the high variability that BL Lacs show, or are moderately bright AGNs whose nonthermal emission does not show evidence of relativistic beaming (see also Massaro et al. 2012c).

3. Investigating Large-scale Environments

The comparison between large-scale environments of BZB, FR I, and LERG samples, all in the SDSS central footprint, is carried out adopting the same procedure of M19 and M20. We used the number of cosmological neighbors to estimate the environmental richness. Cosmological neighbors are defined as all optical sources with SDSS magnitude flags indicating a galaxy-type object and having a spectroscopic z with $\Delta z = |z_{src} - z| \leqslant 0.005$, thus corresponding to the maximum velocity dispersion in groups and clusters of galaxies (see, e.g., Berlind et al. 2006). We indicate the number of cosmological neighbors as N_{cn}^{500} and N_{cn}^{2000}, for those lying within 500 kpc and 2 Mpc from the central source, respectively. Table 1 lists all parameters estimated for each sample analyzed here. In Figure 1 we show the R-band optical image of the field around one BZB and one FR I in our samples, with all cosmological neighbors highlighted.

As previously carried out to compare large-scale environments of two different classes we performed the following statistical tests. The first is based on $\bar{N}_{cn}^{500}$, i.e., medians of the N_{cn}^{500} distribution, while the second applies the Mann–Whitney U statistic. To avoid cosmological effects both tests are performed a redshift bin of 0.01 (see M20 for details).

We also compared the environment of FR 0s with that of BZBs. However, since the FR 0 sample is limited to $z = 0.05$, we simulate how galaxy overdensity surrounding FR 0s would be detected if they lie at larger redshifts, adopting the same strategy of Capetti et al. (2020). Thus, assuming that large-scale environments of FR 0s do not evolve in the redshift range between 0.05 and 0.15, we computed the absolute magnitude in the R band of all cosmological neighbors, and maintaining their

[9] z_{src} indicates the source redshift, while z_{cl} represents a possible nearby galaxy group/cluster.

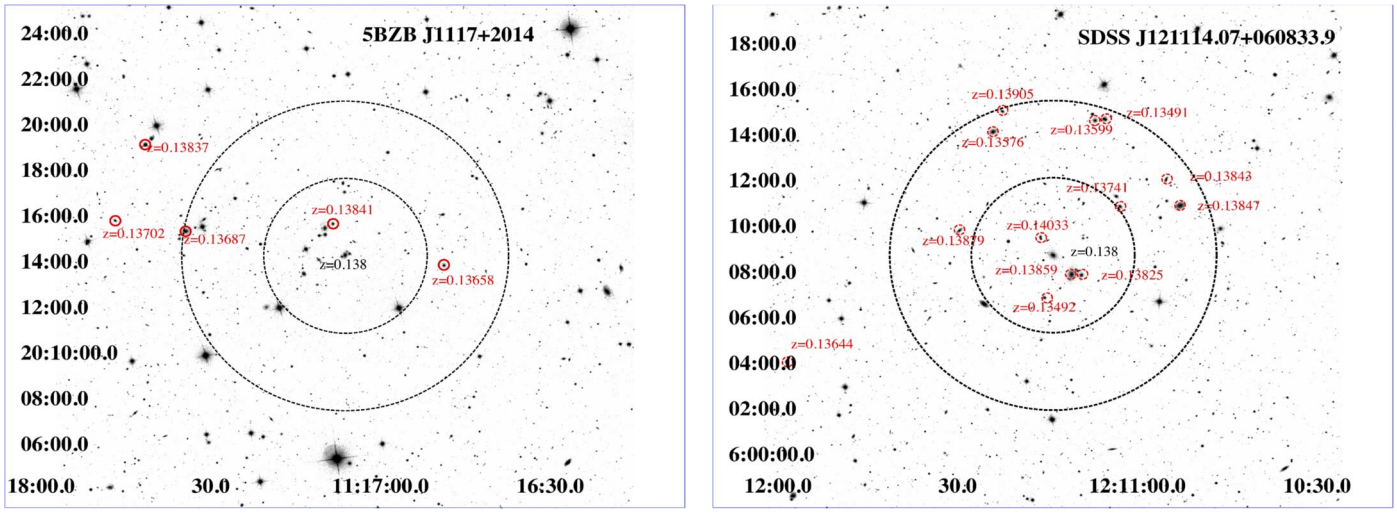

Figure 1. (Left) The *R*-band SDSS image of the field surrounding 5BZB J1117+2024 centered on its position. The two black circles have radii of 500 kpc and 1 Mpc, respectively, computed at the central source redshift. All cosmological neighbors are marked with a red circle and have their $z_{src} <$ reported. In our sample 5BZB J1117+2024 has the largest number of cosmological neighborhoods within 2 Mpc. (Right) Same as left panel for the FR I SDSS J121114.07+0608339 at the same redshift of 5BZB J1117+2024, both reported close to their positions in black. It is quite evident that SDSS J121114.07+0608339 has a large-scale environment that is richer in galaxies than that of 5BZB J1117+2024. In both figures cosmological neighbors are brighter than 17.8 mag in the *R* band (i.e., the SDSS threshold) to select spectroscopic targets.

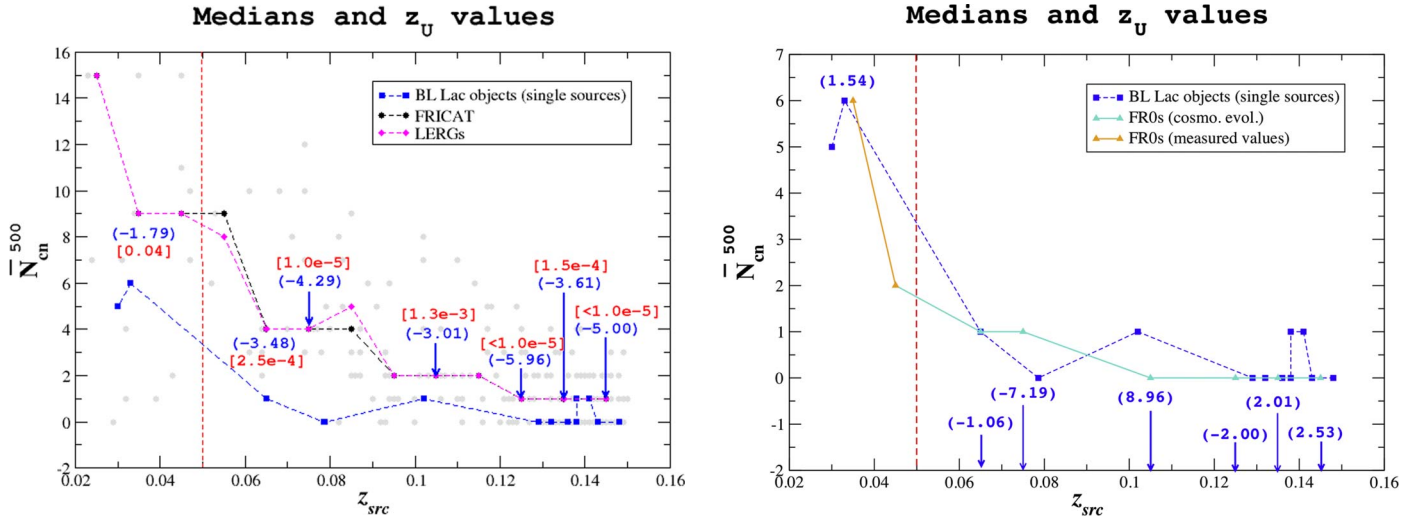

Figure 2. (Left) Medians of N_{cn}^{500} for FR Is (black circles) and LERGs (magenta diamonds) per redshift bins of 0.01 size. The blue square corresponds to the values for single BZBs at $z_{src} < 0.15$. The blue numbers reported in parentheses close to each median of LERGs correspond to values computed for the z_U normalized variable of the Mann–Whitney *U* statistic test performed between BZBs and LERGs (see Section 3 for details), while the red numbers correspond to the *p*-values. As shown BZBs are distributed systematically below all medians of both FR Is and LERGs, thus indicating that they inhabit less galaxy-rich large-scale environments. All gray circles shown in the background correspond to the single values of N_{cn}^{500} for all considered LERGs. (Right) Same as left panel but reporting the comparison between BZBs and FR 0s. Orange triangles are measured medians below $z_{src} = 0.05$, while cyan triangles refer to simulated medians between $0.05 < z < 0.15$ for each bin where there is at least one BZB. It is remarkable that there is agreement between both measured and estimated/simulated medians of the FR 0 population and that of BZBs, indicating that the former could be the parent population of BZBs. Values of the normalized z_U variable are also reported.

intrinsic power, we rescaled it at larger distances, i.e., in all redshift bins where there is at least one BZB. We also recomputed the radii of 500 kpc and 2 Mpc in each redshift bin. We measured the number of cosmological neighbors with a rescaled apparent magnitude m_r brighter than 17.8 corresponding to the SDSS criterion to select spectroscopic targets. These simulations allow us to measure expected medians of cosmological neighbors within 500 kpc and 2 Mpc circles for FR 0s up to $z = 0.15$.

These simulations were tested over the FR I samples. Under the same assumptions we previously described, we computed median values of all cosmological neighbors surrounding simulated FR Is in all redshift bins up to $z = 0.15$ where there is at least one BZB and we found perfect agreement, with the observed values being 4 at $z = 0.065$, 3 at $z = 0.075$, and 1 at $z = 0.105$, 0.125, and 0.135, as reported in the following.

4. Results

The median values $\bar{N}_{cn}^{500}$ for both samples of FR Is and LERGs are shown in Figure 2. It is clear that the measured values of N_{cn}^{500} for all 14 BZBs lying at $z_{src} < =0.15$ all lie systematically below the $\bar{N}_{cn}^{500}$ of both radio galaxy samples.

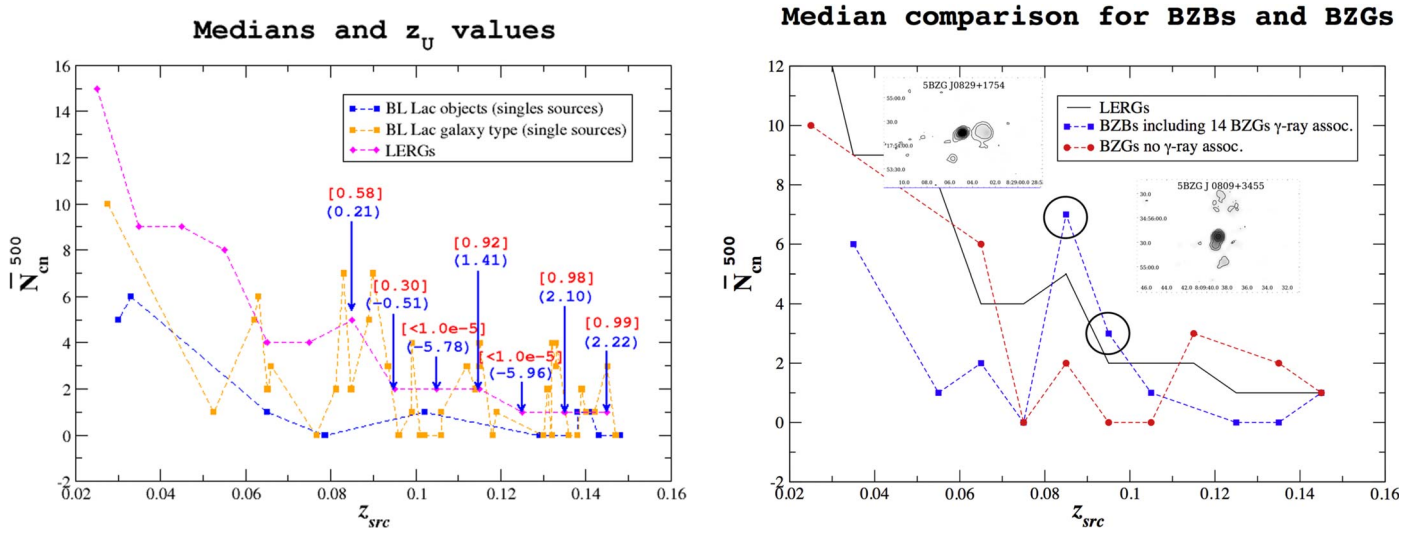

Figure 3. (Left) Same as Figure 2 but comparing BZBs and BZGs. Here it is quite evident that there is agreement between BZGs and LERGs, with the former class being more separated from BZBs. (Right) The comparison between the BZB medians computed including all BZGs associated with γ-ray sources, that are considered weak BZBs, and all remaining BZGs in the original sample. The two black circles highlight z bins where there are mostly BZGs, and that at $z = 0.075$ where the two BZGs clearly show extended radio structures highlighted on the radio maps at 1.4 GHz with coconut levels drawn at 0.0005, 0.0025, 0.125, 0.625 Jy.

Then, comparing $\bar{N}_{\rm cn}^{2000}$ the situation is in agreement with previous results with only 3 out of 14 BZBs for which $\bar{N}_{\rm cn}^{2000}$ is marginally consistent with that of radio galaxies (i.e., FR Is and LERGs).

In Figure 2 we show the two RG distributions of the normalized z_U variable above each $N_{\rm cn}$ median value. These distributions are computed for the Mann–Whitney U test when comparing BZBs with LERGs. This is again systematically negative and not consistent with zero within more than a 3σ level of confidence, with the only exception being a single bin between $z = 0.03$ and $z = 0.04$. The latter statistical tests were performed in each redshift bin, thus grouping BZBs as LERGs.

Both statistical tests allows us to reject the hypothesis that the large-scale environments of BZBs and that of FR Is and/or LERGs are similar with a high level of confidence, and a chance probability of 10^{-4} for the median test. This implies that FR Is, or more generally LERGs, inhabit richer large-scale environments than BZBs and cannot be their "parent" population as predicted by the AGN unification scenario.

Finally, we compared large-scale environments of BZBs and FR 0s where measured values of $\bar{N}_{\rm cn}^{500}$ and $\bar{N}_{\rm cn}^{2000}$ of FR 0s are only available at $z_{\rm src} < 0.05$. However, adopting the simulations described in Section 3 we "extrapolated" the behavior of FR 0 environments up to $z = 0.15$. As shown in Figure 2 values of $N_{\rm cn}^{500}$ for BZBs and FR 0s, both measured (i.e., below $z = 0.05$) and extrapolated up to $z = 0.15$ with the median test and/or using the z_U normalized variable, appear indistinguishable.

5. Comparison with the Literature

Most analyses carried out to date on BZB large-scale environments have been focused on single sources and small samples (see, e.g., Arp 1970; Disney 1974; Craine et al. 1975; Stickel et al. 1991; Rovero et al. 2016; Torres-Zafra et al. 2018), with several being based on photometric companion galaxies in their neighborhoods (Falomo et al. 1990, 1993a, 1993b, 1995; Wurtz et al. 1993; Pesce et al. 1994, 1995; Muriel et al. 2015). However, the findings are controversial and contradictory.

In 2016 a comparison between BZBs listed in the Roma-BZCAT and sources belonging to the catalog of galaxy clusters and groups of Merchàn & Zandivarez (2005) was presented (Muriel 2016). This was the first statistical analysis over a large sample of BL Lacs. Muriel (2016) found that 121 blazars appear to be associated with sources listed in the cluster catalog; Roma-BZCAT classifies them as 24 BZBs, 96 BZGs, and 1 BZU. Restricting the analysis to redshifts below $\sim$0.2, where the cluster catalog is less incomplete, the number of spatial coincidences decreases to 78. Taking into account the contamination by spurious groups/clusters of galaxies, only $43\% \pm 5\%$ of all BL Lac objects, including BZGs, lie in groups of three or more members, where the expected fraction computed for a random sample of galaxies, having the same redshift distribution, is $19.3\% \pm 0.1\%$. Muriel (2016) also applied a correction factor due to the redshift incompleteness of the algorithm used to create the galaxy cluster/group catalog, then claimed a BZB fraction in groups of $\sim 67\% \pm 8\%$ for all 78 sources.

According to Roma-BZCAT, BZGs are not "genuine" blazars, but could be moderately bright AGNs whose non-thermal emission does not show evidence of relativistic beaming and/or are misclassified sources. Thus, we analyzed BZGs analyzed separately from BZBs.

In Figure 3 we compared BZBs and BZGs and found that values of cosmological neighbors for BZGs are consistent with those of radio galaxies. Thus, mixing BZBs with BZGs, given the larger number of BZGs at $z < 0.15$ (i.e., 129 in the Muriel sample) they could bias the whole statistical analysis. Moreover, Muriel (2016) also did not consider any constraint on the "redshift distance" between BZBs and nearby galaxy clusters, thus neglecting spurious association.

To further explore the BZB versus BZG "dichotomy" we assumed that all BZGs associated with a γ-ray source are "real" BZBs with dimmed jet emission below the host galaxy component. Then we double the BZB sample and again run our comparative analysis between them and the LERGs. We found no differences with respect to the previous results, the only exception being one redshift bin centered at 0.075 where there are only two BZGs, 5BZG J0809+3455 and 5BZG J0829 +1754. However, we inspected their FIRST radio maps and

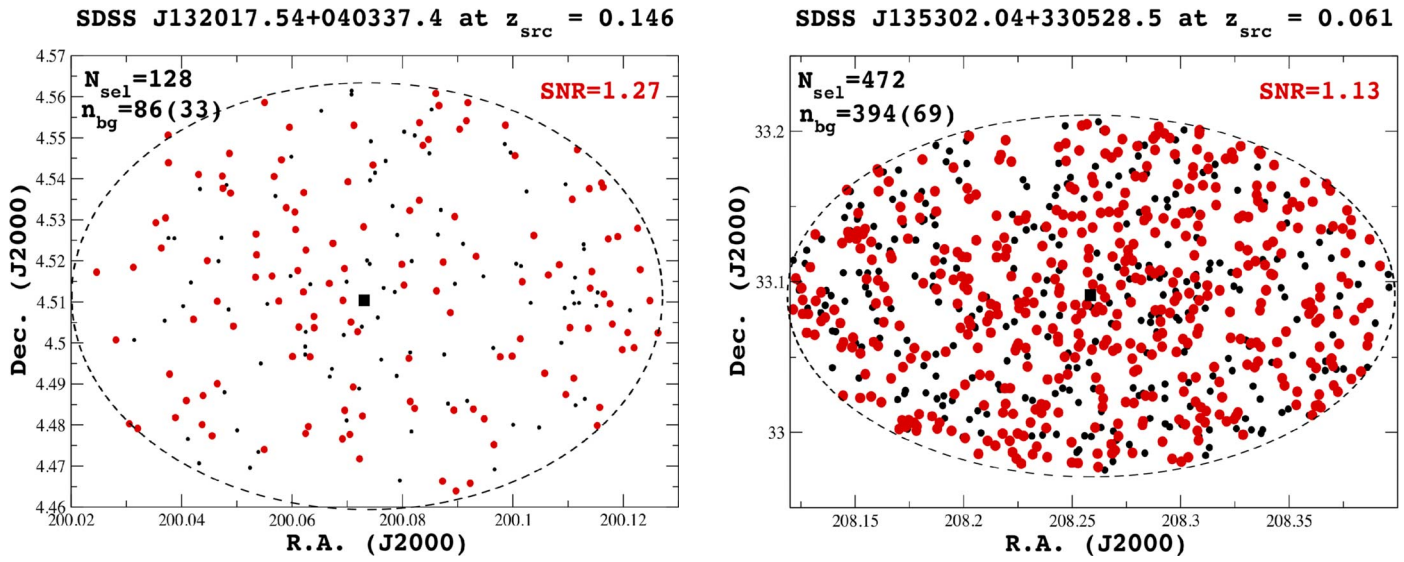

Figure 4. All SDSS sources lying within 500 kpc (black ellipse), computed at the redshift of two FR Is lying in the center of both images: SDSS J132017.54 +043037.4 (left) and SDSS J135302.04+330528.5 (right). The black circles mark sources listed as galaxies according to SDSS flags (see Section 5 for details), while those brighter than the absolute magnitude in the i band equal -21 and computed at the redshift of the central radio galaxy, are red and their number is $N_{\rm sel}$. The number of background galaxies $n_{\rm bg}$ is also reported, with its standard deviation in parentheses in both images, together with the S/N. This number is computed by averaging the galaxy count and adopting the same i-band magnitude selection, over 20 regions of the same area centered at an angular separation greater than 4 Mpc from the central sources. Both measurements clearly show in excess that the galaxy number density $E_r = N_{\rm sel} - n_{\rm bg}$ is consistent with background fluctuations at less than 2σ (i.e., as an upper limit).

they show clear extended radio structures (i.e., lobes and plumes) beyond tens of kiloparsecs, thus making them very different from BZBs and classical LERGs.

An analysis based on similar samples used here, comparing FR Is and BZBs, has been recently carried out (see Sandrinelli et al. 2019 for details) using the average excess of galaxy surface density E_r. As extensively discussed in Massaro et al. (2019, 2020) this method has several statistical and cosmological uncertainties. An analysis performed without removing these biases will show that the higher-redshift population tends to inhabit less galaxy-rich large-scale environments.

Moreover, this method improperly averages measurements of E_r with different signal-to-noise ratios (S/Ns) and compares sources in different redshift bins, thus including cosmological artifacts. To illustrate this S/N effect in Figure 4 we show SDSS sources around two FR Is, namely SDSS J132017.54+043037.4 at $z_{\rm src} = 0.146$ and SDSS J135302.04+330528.5 at $z_{\rm src} = 0.061$, together with all background and foreground galaxies within a circular region of 500 kpc. Surrounding galaxies $N_{\rm sel}$ are selected to have SDSS flags $q\_mode = 1$, $Q > 2$), $cl = 3$ and $ic = 3$ and an absolute magnitude in the i band, computed at the same distance of the central source, greater than -21. The number of background galaxies $n_{\rm bg}$, reported with its standard deviation in parentheses, was estimated adopting the same criteria mentioned above and averaging on 20 regions of the same area centered at an angular separation greater than 4 Mpc from the central source. Both measurements clearly show an excess of galaxies that is marginally significant ($\sim 1\sigma$), consistent with background fluctuations; averaging over these measurements does not appear to be statistically correct. This complicates any comparison with our results.

6. Summary and Conclusions

In the present analysis we focused on a comparison between large-scale environments of BZBs and radio galaxies at similar redshifts. This is the key to obtaining robust results that guarantee avoidance of the statistical biases and cosmological artifacts that affected previous analyses (see Section 5 for a comparison with the literature). Our analysis is carried out by counting the number of cosmological neighbors, i.e., optical galaxies with a firm spectroscopic redshift and with velocities within the maximum velocity dispersion of sources belonging to galaxy groups and clusters.

Our results are summarized as follows.

1. In the local universe the large-scale environment of BZBs is systematically different from that of both FR Is and LERGs, suggesting that the unification scenario of radio-loud AGNs must be revised.
2. However, a direct comparison between the environmental properties of BZBs and the low-power "compact" radio galaxies, known as FR 0s, reveals that their large-scale environments are indistinguishable. This suggests that FR 0s could be the parent population of BZBs.
3. Comparing BZBs and BZGs we found that the latter class appears to have large-scale environments more similar to LERGs, thus it is unlikely they are all "weak" BZBs.
4. Investigations of large-scale environments based on the average excess of galaxy surface density do not appear statistically robust, as they are affected by cosmological artifacts and uncertainties due to the S/N.

We conclude that BZBs are mainly aligned counterparts of compact FR 0s and, only in extreme cases, LERGs. This correspondence between BZBs and FR 0s, both hosted in massive elliptical galaxies, points to the ubiquitous presence of relativistic jets as a natural outcome of gas accretion into the deep gravitational potential well produced by supermassive black holes.

F.M. thanks Dr. C. C. Cheung for their valuable discussions on this project during the organization of the IAU 313

Symposium. This work is supported by the "Departments of Excellence 2018–2022" Grant awarded by the Italian Ministry of Education, University and Research (MIUR) (L. 232/2016). This research made use of resources provided by the Ministry of Education, Universities and Research for the grant MASF_FFABR_17_01. This investigation is supported by the National Aeronautics and Space Administration (NASA) grants GO9-20083X. TOPCAT and STILTS astronomical software (Taylor 2005) were used for the preparation and manipulation of the tabular data and the images.

ORCID iDs

F. Massaro https://orcid.org/0000-0002-1704-9850
A. Capetti https://orcid.org/0000-0003-3684-4275
A. Paggi https://orcid.org/0000-0002-5646-2410
R. D. Baldi https://orcid.org/0000-0002-1824-0411
I. Pillitteri https://orcid.org/0000-0003-4948-6550
R. Campana https://orcid.org/0000-0002-4794-5453

References

Abdollahi, S., Acero, F., Ackermann, M., et al. 2020, ApJS, 247, 33
Aharonian, F., Akhperjanian, A. G., Bazer-Bachi, A. R., et al. 2007, ApJL, 664, L71
Ahn, C. P., Alexandroff, R., Allende Prieto, C., et al. 2012, ApJS, 203, 21
Antonucci, R. R. J., & Ulvestad, J. S. 1985, ApJ, 294, 158
Arp, H. 1970, ApL, 5, 75
Baldi, R. D., Capetti, A., & Giovannini, G. 2015, A&A, 576A, 38
Baldi, R. D., Capetti, A., & Massaro, F. 2018, A&A, 609A, 1
Bennett, C. L., Larson, D., Weiland, J. L., & Hinshaw, G. 2014, ApJ, 794, 135
Berlind, A. A., Frieman, J., Weinberg, D. H., et al. 2006, ApJS, 167, 1
Blandford, R. D., & Rees, M. J. 1978, in Proc. Pittsburgh Conf. on BL Lac Objects (Pittsburgh, PA: Univ. Pittsburgh Press), 328
Capetti, A., Massaro, F., & Baldi, R. D. 2017a, A&A, 598A, 49
Capetti, A., Massaro, F., & Baldi, R. D. 2017b, A&A, 601A, 81
Capetti, A., Massaro, F., & Baldi, R. D. 2020, A&A, 633A, 161
Craine, E. R., Tapia, S., & Tarenghi, M. 1975, Natur, 258, 56
D'Abrusco, R., Massaro, F., Ajello, M., et al. 2012, ApJ, 748, 68
de Menezes, R., Peña-Herazo, H. A., Marchesini, E. J., et al. 2019, A&A, 630, A55
Disney, M. J. 1974, ApJ, 193L, 103
Falomo, R., Melnick, J., & Tanzi, E. G. 1990, Natur, 345, 692
Falomo, R., Pesce, J. E., & Treves, A. 1993a, AJ, 105, 2031
Falomo, R., Pesce, J. E., & Treves, A. 1993b, ApJ, 411L, 63
Falomo, R., Pesce, J. E., & Treves, A. 1995, ApJ, 438L, 9
Fanaroff, B. L., & Riley, J. M. 1974, MNRAS, 167, 31
Healey, S. E., Romani, R. W., Taylor, B. G., et al. 2007, ApJS, 171, 61
Heckman, T. M., & Best, P. N. 2014, ARA&A, 52, 589
Hine, R. G., & Longair, M. S. 1979, MNRAS, 188, 111
Laing, R. A., Jenkins, C. R., Wall, J. V., & Unger, S. W. 1994, in ASP Conf. Ser. 54, The First Stromlo Symp.: The Physics of Active Galaxies, ed. G. V. Bicknell, M. A. Dopita, & P. J. Quinn (San Francisco, CA: ASP), 201
Lister, M. L., Aller, M. F., Aller, H. D., et al. 2013, AJ, 146, 120
Massaro, E., Giommi, P., Leto, C., et al. 2011, Multifrequency Catalogue of Blazars (3rd ed.; Rome: ARACNE Editrice)
Massaro, E., Maselli, A., Leto, C., et al. 2015a, Ap&SS, 357, 75
Massaro, E., Nesci, R., & Piranomonte, S. 2012c, MNRAS, 422, 2322
Massaro, F., Àlvarez-Crespo, N., Capetti, A., et al. 2019, ApJS, 240, 20
Massaro, F., Álvarez Crespo, N., D'Abrusco, R., et al. 2016, Ap&SS, 361, 337
Massaro, F., Capetti, A., Paggi, A., et al. 2020, ApJS, 247, 71
Massaro, F., D'Abrusco, R., Tosti, G., et al. 2012a, ApJ, 752, 61
Massaro, F., D'Abrusco, R., Tosti, G., et al. 2012b, ApJ, 752, 61
Massaro, F., Giroletti, M., Paggi, A., et al. 2013, ApJS, 208, 15
Massaro, F., Thompson, D. J., & Ferrara, E. C. 2015b, A&ARv, 24, 58
Merchàn, M. E., & Zandivarez, A. 2005, ApJ, 630, 759
Muriel, H. 2016, A&A, 591, L4
Muriel, H., Donzelli, C., Rovero, A. C., & Pichel, A. 2015, A&A, 574A, 101
Pavlidou, V., Angelakis, E., Myserlis, I., et al. 2014, MNRAS, 442, 1693
Peña-Herazo, H. A., Massaro, F., Chavushyan, V., et al. 2020, A&A, submitted
Pesce, J. E., Falomo, R., & Treves, A. 1994, AJ, 107, 494
Pesce, J. E., Falomo, R., & Treves, A. 1995, AJ, 110, 1554
Rovero, A. C., Muriel, H., Donzelli, C., & Pichel, A. 2016, A&A, 589A, 92
Sandrinelli, A., Falomo, R., & Treves, A. 2019, MNRAS, 485L, 89
Stickel, M., Padovani, P., Urry, C. M., Fried, J. W., & Kuehr, H. 1991, ApJ, 374, 431
Taylor, M. B. 2005, ASPC, 347, 29
Torres-Zafra, J., Cellone, A. S., Buzzoni, A., Ileana, A., & Portilla, J. 2018, MNRAS, 474, 3162
Urry, C. M., & Padovani, P. 1995, PASP, 107, 803
Villarroel, B., & Korn, A. J. 2014, NatPh, 10, 417
White, R. L., Becker, R. H., Helfand, D. J., & Gregg, M. D. 1997, ApJ, 475, 479
Wurtz, R., Ellingson, E., Stocke, J. T., & Yee, H. K. C. 1993, AJ, 106, 869
Zirbel, E. L. 1997, ApJ, 476, 489
Zou, F., Yang, G., Brandt, W. N., & Xue, Y. 2019, ApJ, 878, 11